J Mater Sci (2011) 46:3027–3045
DOI 10.1007/s10853-010-5181-1

Effects of Sr-modification, iron-based intermetallics and aging treatment on the impact toughness of 356 Al–Si–Mg alloy

O. Elsebaie · A. M. Samuel · F. H. Samuel

Received: 13 July 2010 / Accepted: 9 December 2010 / Published online: 29 December 2010

Abstract Impact toughness as a property has been acquiring increased importance in recent years, since data regarding this property can provide a means for assessing alloy ductility under high rates of deformation. The main objective of this study is to investigate the effects of Sr-modification, Fe-based intermetallic phases and aging conditions on the impact toughness of widely used 356 alloys. The total absorbed energy was measured using a computer-aided instrumented Instron Charpy impact testing machine. Increasing the level of iron additions decreases the impact energy values of 356 alloys to a noticeable degree ($\sim$35–57%). The addition of 0.1 wt% Mn to non-modified 356 alloys seems to have no observable effect on the impact energy, while increasing the Mn addition to 0.4 wt% produces a slight improvement in the impact energy values for non-modified and Sr-modified 356 alloys compared to that of those containing only iron under the same conditions. The application of solution heat treatment in combination with Sr-modification was found to significantly improve the impact energy of as-cast 356 alloys, particularly at low iron additions. Artificial aging of non-modified and Sr-modified 356 alloys at 180 °C diminishes the impact energy values with an increase in the aging time up to 8 h compared to those obtained under the solution heat-treated conditions. On the other hand, aging at 220 °C for 12 h increases the impact energy values of Sr-modified 356 alloy containing 0.12 wt% Fe and combined 0.2 wt% Fe–0.1 wt% Mn to about 20 and 18 J, respectively. The fracture behavior of non-modified 356 alloys containing 0.12 wt% Fe is mainly controlled by the acicular eutectic Si particles whereas β-iron platelets act as crack initiation sites and provide further path for final crack propagation in non-modified 356 alloys containing 0.9 wt% Fe. The β-iron platelets and π-iron phase particles contribute largely to crack initiation and propagation in the Sr-modified 356 alloys containing 0.9 wt% Fe.

O. Elsebaie · A. M. Samuel · F. H. Samuel (✉)
Université du Québec à Chicoutimi, Chicoutimi, QC, Canada
e-mail: fhsamuel@uqac.ca

F. H. Samuel
College of Engineering, King Saud University,
Riyadh,
Saudi Arabia

F. H. Samuel
Center of Excellence for Research in Engineering Materials,
Riyadh, Saudi Arabia

Introduction

Conflicting requirements with respect to decreasing vehicle weight while at the same time increasing its crashworthiness present a major challenge to designers in automotive industry. Aluminum alloys are now established as lightweight materials providing excellent weight-saving potential and crash resistance for passive vehicle safety. The 356-group of aluminum alloys is considered to be the most popular type among Al–Si–Mg alloy systems. Due to economic and environmental requirements, it is becoming increasingly important to reduce vehicle weight. For such an objective, 356 alloys have been commercially used to produce diesel engines, cylinder heads, and vehicle wheels because of their high strength-to-weight ratio, high castability, and thermal expansion coefficient, together with high wear and corrosion resistance values.

The impact toughness of Al–Si alloys is regulated to a high degree by their microstructure which depends significantly not only on alloy chemistry, melt treatment

processes, and solidification conditions but also on heat treatment. Depending on the alloy chemical composition and solidification conditions, the microstructure of 356 alloys usually consists of α-Al dendrites, eutectic Si particles, and variety of intermetallic phases. Some of these intermetallic phases, such as Mg_2Si, improve the strength values of such alloys through the precipitation-hardening which occurs during the application of a T6 temper, whereas others, like the Fe-bearing intermetallic phases, have a deleterious effect on mechanical properties. The β-Al_5FeSi iron intermetallic phase is considered to be one of the most detrimental iron-based intermetallic phases, in which the plate-like morphology of this phase creates potential crack initiation sites and ultimately leads to the impairment of the ductility and fracture toughness of these Al–Si alloys [1].

The design of certain critical components to meet specific service requirements is of importance in the automobile industry. Impact toughness is one of the main requirements which should be taken into account in the design of such automobile components. In this way, sudden failure resulting from weakened impact toughness may be circumvented through the selection of the proper alloy composition and the appropriate casting and heat treatment conditions.

In this study, the influence of individual additions of Fe or combined Fe–Mn additions on the impact toughness was investigated concomitantly with aging conditions, to acquire a clear understanding of this essential property, in order to reach a balanced compromise between the behavior of both impact toughness and hardness. The findings of this study will facilitate in designing and selecting the proper chemical composition and heat treatment suitable for 356 alloys in order to meet the service conditions required for castings.

Experimental procedures

The as-received ingots of 356 alloy which has a chemical composition presented in Table 1 were melted using an electric induction furnace and the melting temperature was maintained at 730 ± 5 °C. The molten metal was degassed using pure dry argon injected into the molten metal by means of a rotary degassing impeller made of graphite. All the molten alloys were grain-refined after degassing, using Al–5 wt% Ti–1 wt% B master alloy. The molten metal was poured into an L-shaped preheated permanent steel mold giving a dendrite arm spacing (SDAS) of 45 μm. The castings obtained for the 356 alloys were machined and milled, then cut into three rectangular blocks for hardness measurements in the as-cast, solution heat treatment and aging conditions. The full heat treatment process was performed using blue M forced-air electric furnace, model SPX, equipped with a programable temperature controller (±1 °C), as summarized in Table 2. After hardness measurements, each block were cut into four bars in which each four bars represent each alloy/heat treatment condition. These bars were then milled to get the exact specimen dimensions (10 × 10 × 55 mm) for the Charpy impact test corresponding to the ASTM E23 standard specifications. Since Al alloys are fragile and low toughness material, it decided to use an unnotched test specimen to emphasize on the dependence of the Charpy impact energy values on the metallurgical parameters rather than on the specimen configuration. The surfaces of the impact-tested specimens were polished with sandpaper to remove any irregularities and scratches resulting from the milling process.

Charpy impact testing was performed on unnotched test specimen extracted from the 356 alloys investigated in the as-cast and heat-treated conditions as listed in Table 2. This testing was carried out using an Instron Charpy Impact Testing machine, model SI-1D3 from SATEC Systems Inc. Data acquisition system was connected to the pendulum of the impact machine so as to monitor the behavior of the test specimen by measuring the load, total impact energy, crack initiation energy, and crack propagation energy.

An Olympus optical microscope was used to examine the microstructure and also to study both the fracture profile and the components of microstructure involved in the crack formation occurring on and below the surface of metallographic samples which were sectioned off perpendicular to the fracture surface. A JEOL JXA-8900L

Table 1 Classification of 356 alloys used in this study

Alloy	Alloy code	Chemical composition and additives	Heat treatment procedures
356	A	(Al–7%Si–0.35%Mg) + 0 Fe	SHT 8 h at 540 °C
	B	(Al–7%Si–0.35%Mg) + 0.2 Fe	Quenching in warm water (65 °C)
	C	(Al–7%Si–0.35%Mg) + 0.4 Fe	Aging at 25 °C for 24 h
	D	(Al–7%Si–0.35%Mg) + 0.8 Fe	Aging at 180 °C, 220 °C for 2, 4, 6, 8, 12 h
	E	(Al–7%Si–0.35%Mg) + 0.2 Fe + 0.1 Mn	
	F	(Al–7%Si–0.35%Mg) + 0.4 Fe + 0.2 Mn	
	G	(Al–7%Si–0.35%Mg) + 0.8 Fe + 0.4 Mn	

Table 2 Chemical composition of 356 alloys used in this study

Alloy code	Elements (wt%)								
	Si	Mg	Cu	Fe	Mn	Ti	Sr	Mn/Fe	Bal.
A[a]	6.5	0.27	0.03	0.11	0.03	0.09	0.00	0.293	92.8
AS[a]	6.9	0.33	0.14	0.14	0.03	0.1	0.017	0.246	92.1
B	6.7	0.25	0.017	0.25	0.03	0.1	0.00	0.134	92.5
BS	7.08	0.34	0.17	0.23	0.04	0.11	0.014	0.179	91.9
C	6.7	0.31	0.017	0.43	0.03	0.1	0.00	0.081	92.2
CS	6.5	0.36	0.06	0.35	0.002	0.14	0.014	0.007	92.5
D	6.8	0.3	0.017	0.87	0.03	0.10	0.00	0.04	91.8
DS	6.8	0.35	0.045	0.92	0.01	0.14	0.016	0.12	91.6
E	6.4	0.33	0.005	0.24	0.1	0.14	0.00	0.43	92.7
ES	7.6	0.36	0.044	0.22	0.13	0.11	0.017	0.62	91.3
F	6.5	0.31	0.008	0.44	0.2	0.13	0.00	0.472	92.3
FS	7.1	0.35	0.027	0.37	0.2	0.11	0.017	0.614	91.6
G	6.5	0.3	0.015	0.85	0.41	0.11	0.00	0.484	91.7
GS	6.9	0.32	0.029	0.9	0.41	0.11	0.018	0.465	91.1

[a] A: 356 base alloy; S: Sr-modified

model electron probe micro analyzer (EPMA) equipped with a built-in software to calculate the total surface fraction of all intermetallics present in the alloys investigated based on the brightness of the phase.

Results and discussion

It is clear that both the structural fineness and the morphology of the microstructural constituents govern the alloy ductility and hence impact toughness to a large degree. These constituents often include α-aluminum dendrites, the eutectic Si phase, and a variety of interdendritic intermetallic phases. The size, morphology, and distribution of the hardening phases formed during aging treatment are strongly controlled by the aging treatment conditions applied.

Microstructure

The examination of the alloys microstructure makes it possible to better understanding the complex process–structure–property inter-relationship and would, therefore, also help in the assessment of the performance of Al–Si casting components under a variety of service conditions. The main constituents of the microstructure of the 356 alloys investigated will be presented in terms of a qualitative study obtained by means of optical micrographs. In addition, quantitative measurements of the total volume fraction of all intermetallic phases present in the microstructure were carried out for non-modified and Sr-modified alloys under as-cast and solution heat-treated conditions.

Iron-based intermetallic phases

It will be noted, from Fig. 1, that the β-Al_5FeSi phase appears in the form of randomly distributed needles when observed in a two-dimensional optical micrograph, whereas it assumes a plate-like morphology when viewed in three-dimension by means of a scanning electron microscope. The π-$Al_9FeMg_3Si_6$ phase is often observed to be closely connected to/nucleated on the β-phase platelets, forming distinctive platelet particles, as shown in Fig. 1a. This iron intermetallic phase is also observed to form independent script-like particles, as shown in Fig. 1b. This observation may suggest that, as a result of the peritectic reaction, the π-iron phase appears to precipitate during solidification at a temperature just after the formation temperature of the

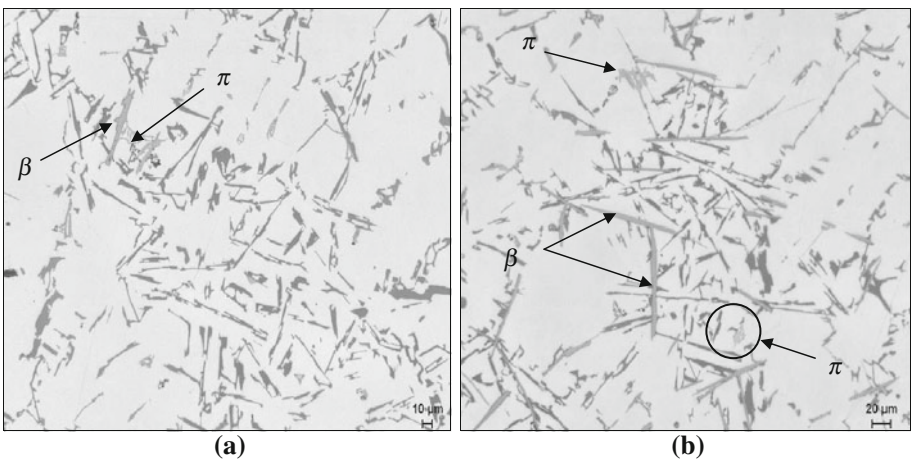

Fig. 1 Optical micrographs showing the formation of β-Al_5FeSi and π-Al_8FeMg_3Si6 iron intermetallic phases present in the as-cast microstructure of the non-modified 356 alloy containing: **a** 0.1 wt% Fe, **b** 0.9 wt% Fe

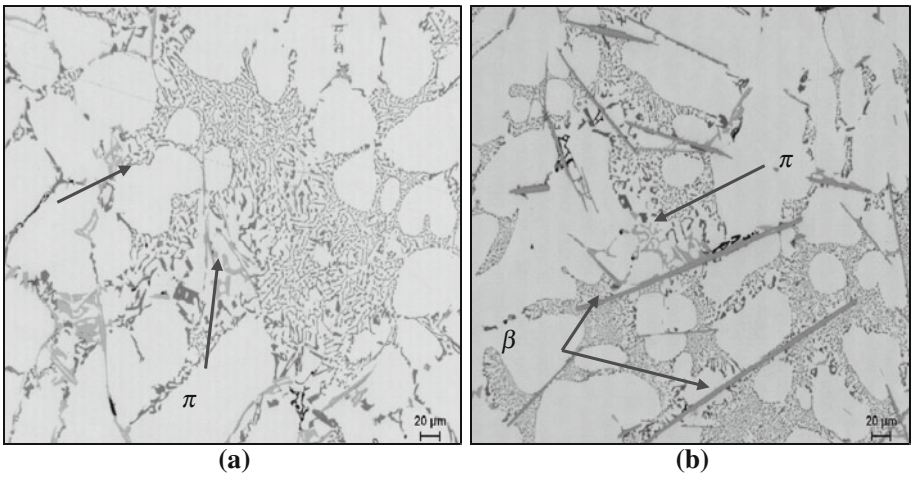

Fig. 2 Optical micrographs showing the segregation of both β- and π-iron intermetallic phases away from the eutectic Si regions in the as-cast microstructure of Sr-modified 356 alloys containing: **a** 0.1 wt% Fe and **b** 0.8 wt% Fe

β-Al_5FeSi platelets [2]. These findings are in agreement with those obtained in a study carried out by Taylor [3] on the effects of iron in Al–Si alloys. The results reveal that the π-iron phase may grow in close association with the β-iron phase platelets or else that it may precipitate in the form of independent script-like particles in the case of as-cast alloys. Figure 2 shows the as-cast microstructures of Sr-modified 356 alloys containing 0.12 and 0.9 wt% iron (AS and DS alloys). It will be observed that both β-iron needles and π-iron script-like particles seem to be segregated away from the regions of eutectic Si colonies in the presence of Sr. It is also worth noting, from Fig. 2, that both of these iron-based phases acquire large-size particles, particularly in the DS alloy (0.9 wt% Fe).

Effect of solution heat treatment

As frequently reported in a number of earlier studies [4–6], the eutectic Si phase is observed to undergo shape changes after solution heat treatment of the 356 alloys are at 540 °C for 8 h, as may be seen clearly in Fig. 3. The fine Chinese script Mg_2Si phase which usually found in the interdendritic regions of the as-cast microstructure is not observed to be present after applying the solution treatment, which confirms their complete dissolution in the α-aluminum solid solution. The small-sized particles of the π-$Al_8FeMg_3Si_6$ phase tended to disappear during solution treatment for the alloys containing 0.12 wt% Fe (A alloy), most likely as a result of their complete dissolution in the matrix. This π-phase may also decompose by releasing its Mg and Si into the aluminum solid solution, leading to its transformation into clusters of fine-scale needles of a Mg-free iron-bearing intermetallic phase, as shown appearing inside the circled areas in Fig. 3a. This newly formed phase is thought to possess a composition similar to that of the β-iron phase [7, 8].

Both the script-like and block-like π-phase forms, which are present in D alloy (0.9 wt% Fe), appear to partially dissolve into the matrix after solution treatment because they acquire large-size particles, as shown inside the circled area in Fig. 3b. It may thus be concluded that the large particles of π-phase seem to be predominantly resistant to changes during solution treatment. The solution heat treatment time at 540 °C appears to be insufficient to either overcome the low diffusivity of iron in solid aluminum or to complete the decomposition of these coarse π particles. The above observations emphasize on the fact that both solution heat treatment conditions and alloy composition are the main parameters controlling the dissolution and/or transformation of the π-phase to a large degree; they are also in good agreement with the results obtained in a study carried out by Wang and Davidson [9] on the solidification and precipitation behavior of Al–Si–Mg alloys.

Figure 4 shows quantitative measurements of the total surface fraction of the intermetallic phases present in the as-cast and solution-treated microstructures of a 356 alloy containing various levels of iron. It is obvious that solution heat treatment results in reducing the total surface fraction of the intermetallic phases for both non-modified and Sr-modified alloy conditions. The apparent absence of particles of the Mg_2Si phase in Fig. 3 confirms the complete dissolution of this phase after solution treatment.

Such a reduction in the total surface fraction of the intermetallics supports the conclusions which were drawn regarding the dissolution and transformation of the π-iron phase, as may be observed from the optical micrographs shown in Fig. 3. The transformation of the π-phase into fine β needles also confirms the drop in the total surface fraction of intermetallics considering that the π-phase is less dense and occupies a larger volume fraction than that of the β-phase. It is worth noting that the total surface fraction of intermetallic phases appears to increase with an increase in the level of iron content, regardless of alloy conditions.

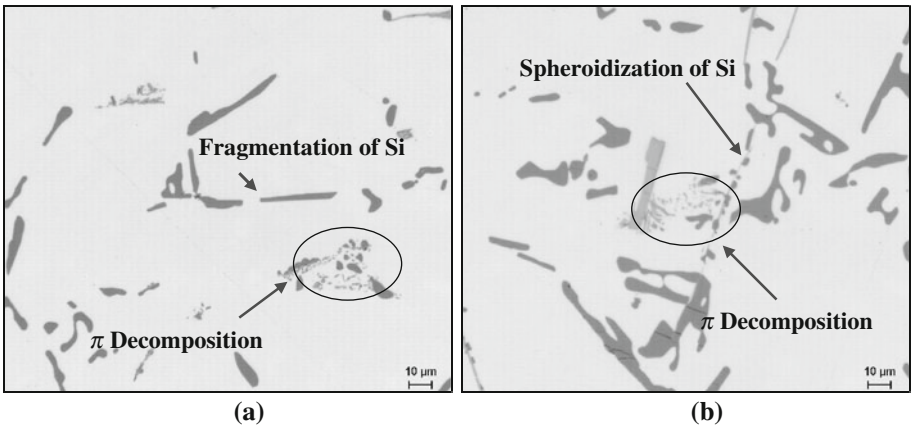

Fig. 3 Optical micrographs of non-modified solution heat-treated 356 alloys containing: **a** 0.1 wt% Fe and **b** 0.8 wt% Fe, showing decomposition of the π-phase and the formation of small new β needles in the microstructure

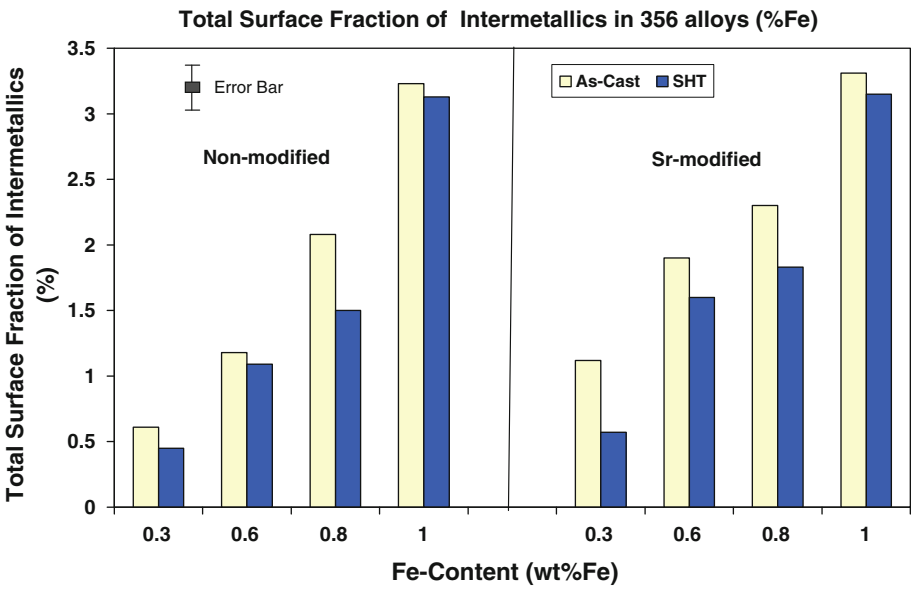

Fig. 4 Effects of solution heat treatment and Fe content on the total surface fraction of intermetallic phases observed in an as-cast 356 alloy for the non-modified and Sr-modified cases

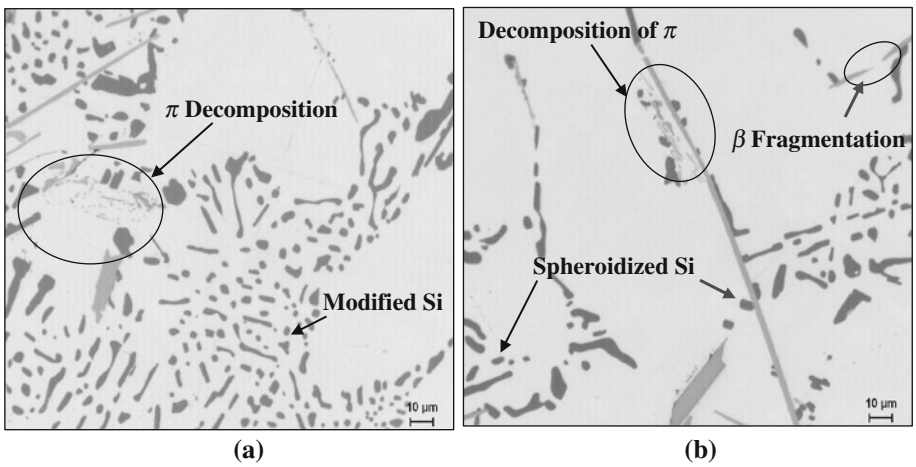

Fig. 5 Optical micrographs of Sr-modified solution heat-treated 356 alloys containing: **a** 0.1 wt% Fe and **b** 0.8 wt% Fe, showing the decomposition of the π-phase and the formation of small new β needles in the microstructure

Similar observations were made in the case of solution heat-treated AS and DS alloys, as shown in Fig. 5. It will also be observed that there are a number of thin β needles which become elongated to the point of necking; they then begin to manifest various states of breakdown, disintegrating into smaller segments, as shown inside the oval area in Fig. 5b.

Impact toughness

Effects of the Fe additions

The effects of the addition of iron, solution heat treatment, and Sr-modification on the impact energy and related parameters obtained for the 356 alloy are listed in Table 3. The scale the Charpy impact energy axis (Y-axis) in the plotted graphs for is varied with the objective of revealing the effects of all parameters involved on the impact behavior. The absorbed impact energy values appear to decrease considerably with an increase in the iron content from 0.12 to 0.9 wt% Fe for all the 356 alloys conditions, as shown in Fig. 6. Increasing the volume fraction of the harmful β-iron platelets with increasing iron content provides more potential sites for crack nucleation and thus facilitates the initiation of cracks which may explain the reduction in the impact energy values. These findings are in fairly satisfactory concurrence with a previous study carried out by Ma et al. [10] on the effects of Fe content on the impact toughness of 356 alloys. Their results revealed that, regardless of the cooling rate, the lowest iron-containing alloys display the highest impact energy values, particularly in the case of the Sr-modified alloys.

With the addition of Sr to the 356 alloys, the morphology of the eutectic Si phase changes to a fibrous form, leading to a reduction in the number of crack initiation sites in the matrix. As a result, the impact values show an improvement, e.g., from 6.4 to 7 J for A and AS alloys, respectively. Such improvement may be a result of the increase in the energy for crack initiation in the matrix, regardless of the level of iron content. This improvement, however, seems to be fairly slight because of the apparent increase in the level of porosity in the microstructure associated with the addition of Sr; this increase in porosity may be considered one of the main disadvantages of using Sr as a modifying agent for Al–Si alloys [11].

Table 3 Effects of Sr-modification and solution heat treatment on Charpy impact energy values of as-cast non-modified 356 alloys

Alloy code	Alloy condition	E_T (J)	E_I (J)	E_P (J)	Time to failure (ms)	ACS (mm/ms)
A	1[a]	6.40 ± 0.6	3.83 ± 0.4	2.57 ± 0.2	0.35 ± 0.02	28.6 ± 1.4
	2[a]	12.48 ± 1	8.55 ± 0.8	3.93 ± 0.4	0.53 ± 0.06	18.8 ± 2.2
B	1	5.50 ± 0.5	3.09 ± 0.3	2.41 ± 0.1	0.34 ± 0.03	29.4 ± 2.2
	2	9.17 ± 0.9	5.63 ± 0.6	3.54 ± 0.3	0.42 ± 0.02	23.8 ± 1
C	1	4.56 ± 0.3	2.46 ± 0.1	2.10 ± 0.2	0.31 ± 0.01	32 ± 1.5
	2	6.13 ± 0.8	3.40 ± 0.5	2.73 ± 0.3	0.35 ± 0.04	28.6 ± 3.6
D	1	3.72 ± 0.2	1.95 ± 0.4	1.77 ± 0.3	0.28 ± 0.03	36 ± 3.3
	2	5.3 ± 0.8	2.78 ± 0.4	2.52 ± 0.3	0.29 ± 0.02	34.5 ± 2.4
E	1	5.35 ± 0.8	2.80 ± 0.3	2.55 ± 0.6	0.29 ± 0.03	34.5 ± 2.8
	2	10.03 ± 0.9	6.20 ± 1	3.83 ± 0.1	0.45 ± 0.01	22.2 ± 1.1
F	1	5.05 ± 0.5	2.86 ± 0.1	2.19 ± 0.1	0.31 ± 0.02	32.2 ± 1.6
	2	9.0 ± 0.4	5.0 ± 0.2	4 ± 0.1	0.42 ± 0.02	23.8 ± 1.6
G	1	4.63 ± 0.5	2.5 ± 0.6	2.13 ± 0.3	0.34 ± 0.03	29.4 ± 2.1
	2	5.99 ± 0.9	3.0 ± 0.4	2.99 ± 0.4	0.33 ± 0.02	30.3 ± 2.4
AS[a]	1	7.00 ± 0.9	3.6 ± 0.5	3.4 ± 0.4	0.38 ± 0.02	26.3 ± 2.1
	2	13.9 ± 0.9	9.17 ± 0.9	4.73 ± 0.3	0.54 ± 0.04	18.5 ± 1.6
BS	1	5.77 ± 0.6	3.2 ± 0.4	2.57 ± 0.4	0.37 ± 0.02	27 ± 2.6
	2	13.7 ± 0.9	9.22 ± 1	4.48 ± 0.2	0.51 ± 0.03	19.6 ± 1.2
CS	1	5.57 ± 0.9	3.10 ± 0.6	2.47 ± 0.2	0.37 ± 0.01	27 ± 3.6
	2	11.97 ± 0.8	7.75 ± 0.8	4.22 ± 0.3	0.54 ± 0.05	18.5 ± 1.8
DS	1	4.53 ± 0.1	2.47 ± 0.2	2.06 ± .08	0.32 ± 0.02	31 ± 1.9
	2	7.22 ± 0.3	3.86 ± 0.3	3.36 ± .09	0.35 ± 0.01	28.5 ± 0.8
ES	1	8.69 ± 0.30	5.12 ± 0.9	3.57 ± 0.3	0.40 ± 0.06	25 ± 3.3
	2	12.51 ± 0.3	6.64 ± 0.9	5.87 ± 0.3	0.54 ± 0.02	18.5 ± 1.3
FS	1	8.41 ± 0.2	4.93 ± 0.5	3.48 ± .09	0.46 ± 0.03	21 ± 1.7
	2	11.31 ± 0.9	6.8 ± 0.6	4.51 ± 0.6	0.53 ± 0.04	18.8 ± 1.1
GS	1	5.45 ± 0.6	3.03 ± 0.3	2.42 ± 0.2	0.37 ± 0.04	27 ± 3
	2	6.67 ± 0.9	3.62 ± 0.9	3.05 ± 0.4	0.34 ± 0.03	29.4 ± 3.2

[a] 1: as-cast; 2: solution heat-treated; S: Sr-modified; E_T: total impact energy; E_I: energy for crack initiation; E_P energy for crack propagation; and ACS: average speed of crack propagation

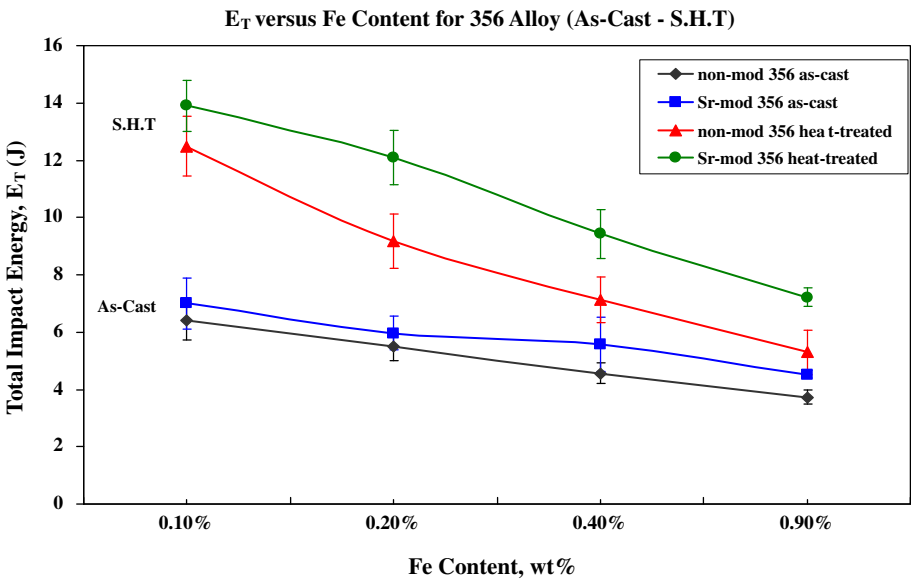

Fig. 6 Total impact energy as a function of Fe content for non-modified and Sr-modified 356 alloys in the as-cast and solution heat-treated conditions

The solution heat treatment at 540 °C for 8 h followed by natural aging for 24 h at room temperature (T4 temper) significantly improves the impact energy values of both A and AS alloys; this represents an increase of about 95 and 117%, respectively (Table 3). The improvement observed in the impact values after the application of the T4 temper is in accordance with the results obtained from the work of Shivkumar et al. [12] on the impact properties of A356 alloys. Their results reveal that the application of solution treatment at 550 °C for a relatively short solution time, e.g., 2 h, is capable of producing a considerable enhancement in the impact energy values of both non-modified and Sr-modified alloys.

With the object of evaluating the impact behavior of 356 alloys, the individual or combined effects of the application of Sr-modification and solution heat treatment on such behavior may be analyzed based on the fracture mechanism of the alloys under investigation. The fracture process of Al–Si alloys consists mainly of two components, the initiation of microcracks and the propagation of these cracks to form the final fracture. Microcracks are often initiated at the sites or regions of high stress concentrations present in the matrix. For Al–Si alloys, these sites are likely to have originated at the sharp edges found at the extremity of acicular Si particles and β-iron platelets as well as at the interface between the precipitate phase particles and the matrix. According to the chemical composition of the alloys investigated and the conditions involved in this study, such sources for crack initiation are expected to be present in the matrix in large amounts. The purpose of Sr-modification, in this instance, is mainly to eliminate the area of high stresses located at the extremities of Si particles and β-iron platelets. The slight increase observed in the impact values of 356 alloys after Sr-modification, however, makes it possible to conclude that the morphology of the eutectic phase, in this case, is not the only parameter controlling impact behavior. Also, there is still the role of iron-based intermetallic phases which should be taken into consideration.

The application of solution heat treatment contributes significantly to further decreasing the number of crack initiation sites through the spheroidization of eutectic Si particles, the dissolution of the brittle Mg_2Si phase, and the fragmentation of β-iron platelets as well as the transformation of the π-iron phase, as may be seen in the optical micrographs shown in Fig. 5. All these microstructural changes appear to improve the crack initiation resistance (CIR) of the matrix.

The propagation of microcracks in the matrix is essentially governed by the ductility of the matrix to a great degree. Increasing the proportion of ductile α-Al phase in the matrix would certainly improve its resistance to crack propagation where the presence of large ligaments of this ductile matrix may act as an effective barrier to the advance and continuity of crack growth. The proportion of ductile α-Al phase in the matrix may be increased through (i) the addition of Sr which depresses the eutectic temperature [13], and (ii) the application of solution treatment leading to an increase in the inter-particle spacing which associated with the spheroidization and coarsening of the eutectic Si phase [12, 14, 15]. It is thus reasonable to presume that applying Sr-modification together with solution heat treatment result in significant improvements in the impact energy values.

The impact properties of 356 alloys are strongly regulated by the morphology and size of both eutectic Si and Mg_2Si phases as well as the iron-based intermetallic compounds. It is evident from the values of the impact

Table 4 Effects of Sr-modification and aging times on Charpy impact energy values of 356 alloys containing four levels of Fe, and aged at 180 °C

Alloy code	Aging time (h)	E_T (J)	E_I (J)	E_P (J)	Time to failure (ms)	ACS (mm/ms)
A	2	8.35 ± 0.9	4.7 ± 0.6	3.65 ± 0.7	0.34 ± 0.02	29.4 ± 2
	4	7.4 ± 0.6	4.0 ± 0.4	3.4 ± 0.5	0.31 ± 0.02	32.2 ± 1.5
	6	6.1 ± 0.4	3.2 ± 0.3	2.9 ± 10.4	0.28 ± 0.01	35.7 ± 1.3
	8	4.9 ± 0.7	2.5 ± 0.4	2.4 ± 0.6	0.26 ± 0.02	40 ± 2.3
	12	5.5 ± 0.8	2.4 ± 0.5	3.1 ± 0.3	0.26 ± 0.03	38.5 ± 3.7
AS	2	9.7 ± 0.9	5.6 ± 0.5	4.1 ± 0.7	0.36 ± 0.03	27.7 ± 2
	4	5.7 ± 0.4	2.8 ± 0.2	2.9 ± 0.5	0.30 ± 0.01	33.3 ± 0.9
	6	5.6 ± 0.5	2.8 ± 0.4	2.8 ± 0.8	0.34 ± 0.03	29.4 ± 3.3
	8	5.5 ± 0.3	2.55 ± 0.1	2.95 ± 0.3	0.31 ± .02	32.2 ± 2.1
	12	7.5 ± 0.8	4.1 ± 0.4	3.4 ± 0.2	0.27 ± 0.02	37.1 ± 2.5
B	2	4.15 ± 0.6	2.08 ± 0.6	2.07 ± 0.7	0.26 ± 0.03	38.5 ± 4
	4	3.82 ± 0.3	1.90 ± 0.2	1.92 ± 0.5	0.24 ± 0.01	41.6 ± 1
	6	4.64 ± 0.3	2.28 ± 0.2	2.36 ± 0.6	0.26 ± 0.01	38.5 ± 0.9
	8	4.34 ± 0.6	2.24 ± 0.4	2.1 ± 0.4	0.26 ± 0.02	38.5 ± 2.7
	12	5.08 ± 0.9	3.76 ± 0.5	1.32 ± 0.3	0.27 ± 0.01	37 ± 0.7
BS	2	7.67 ± 0.7	4.2 ± 0.4	3.47 ± 0.1	0.31 ± 0.01	32.2 ± 1.6
	4	5.83 ± 0.5	3.18 ± 0.4	2.65 ± 0.3	0.30 ± 0.02	33.3 ± 2.3
	6	5.42 ± 0.9	2.86 ± 0.5	2.56 ± 0.5	0.29 ± 0.01	34.5 ± 1.8
	8	5.27 ± 0.3	2.95 ± 0.3	2.32 ± 0.8	0.29 ± 0.03	34.5 ± 3.4
	12	6.4 ± 0.6	3.55 ± 0.4	2.85 ± 0.4	0.28 ± 0.02	35.7 ± 2.14
C	2	3.44 ± 0.7	1.62 ± 0.3	1.82 ± 0.9	0.24 ± 0.01	41.6 ± 1.6
	4	3.05 ± 0.3	1.43 ± 0.1	1.62 ± 0.2	0.22 ± 0.01	45.5 ± 0.5
	6	3.04 ± 0.9	1.66 ± 0.3	1.38 ± 0.5	0.24 ± 0.02	41.6 ± 3.2
	8	2.74 ± 0.2	1.31 ± 0.1	1.43 ± 0.4	0.22 ± 0.01	45.5 ± 2
	12	4.76 ± 0.4	2.38 ± 0.1	2.38 ± 0.2	0.25 ± 0.01	40 ± 1.1
CS	2	6.24 ± 0.8	3.14 ± 0.5	3.10 ± 0.4	0.28 ± 0.02	35.7 ± 3
	4	5.8 ± 0.8	3.1 ± 0.6	2.7 ± 0.3	0.28 ± 0.02	35.7 ± 3.5
	6	5.1 ± 0.3	2.9 ± 0.2	2.2 ± 0.7	0.30 ± 0.01	33.3 ± 0.5
	8	5.15 ± 0.9	3.42 ± 0.4	1.73 ± 0.6	0.26 ± 0.02	38.5 ± 2.6
	12	6.65 ± 0.9	3.77 ± 0.5	2.88 ± 0.2	0.34 ± 0.03	29.4 ± 3.3
D	2	3.03 ± 0.3	1.5 ± 0.2	1.53 ± 0.7	0.22 ± 0.01	45.5 ± 0.6
	4	2.31 ± 0.2	1.2 ± 0.1	1.11 ± 0.8	0.24 ± 0.02	41.6 ± 3.5
	6	2.47 ± 0.5	1.14 ± 0.3	1.33 ± 0.3	0.22 ± 0.01	45.5 ± 2.4
	8	2.51 ± 0.3	1.8 ± 0.2	0.71 ± 0.5	0.22 ± 0.02	45.5 ± 2.6
	12	2.55 ± 0.7	1.2 ± 0.3	1.35 ± 0.4	0.23 ± 0.02	43.5 ± 3.4
DS	2	4.07 ± 0.4	1.95 ± 0.2	2.12 ± 0.3	0.25 ± 0.01	40 ± 2
	4	2.82 ± 0.2	1.36 ± 0.1	1.46 ± 0.4	0.26 ± 0.03	38.5 ± 3
	6	3.09 ± 0.4	1.48 ± 0.2	1.61 ± 0.5	0.24 ± 0.01	41.6 ± 2.3
	8	2.9 ± 0.3	1.36 ± 0.1	1.54 ± 0.1	0.25 ± 0.03	40 ± 3.5
	12	4.86 ± 0.9	2.47 ± 0.6	2.39 ± 0.8	0.23 ± 0.03	43.5 ± 2.3

energies listed in Table 4 that aging at 180 °C for aging time varying from 2 to 8 h reveals a negative effect on the impact behavior, as is also shown in Fig. 7. This observation is evident from a comparison of Figs. 6 and 7 which show clearly the beneficial effect of solution heat treatment. These results are, in fact, to be expected since the aging treatment (T6 temper) is often applied to improve the strength of as-cast 356 Al–Si–Mg alloys through precipitation-hardening of Mg_2Si phase, at the expense of ductility. The coherent β'-Mg_2Si precipitated phase particles with their needle-like shape impede the motion of dislocations leading to an increased buildup of these

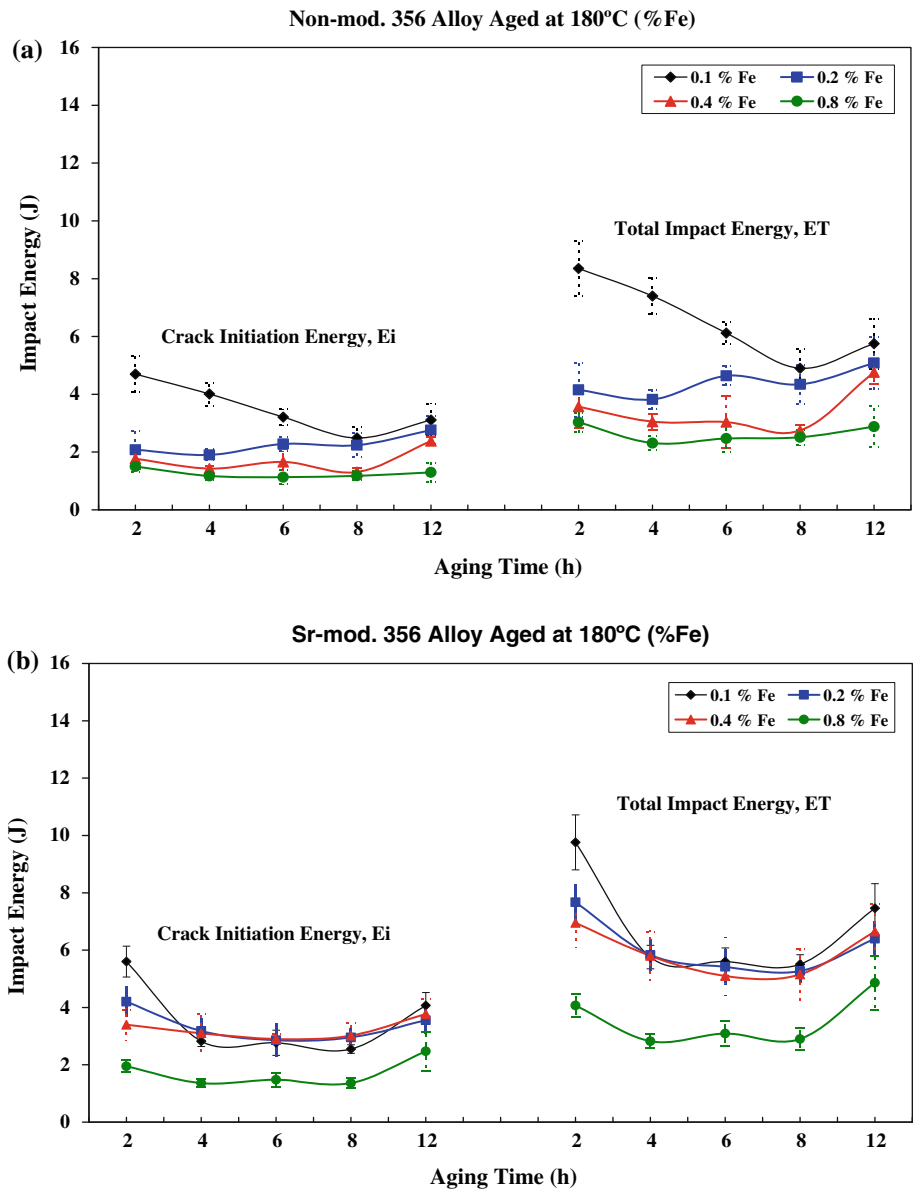

Fig. 7 Impact energy as a function of aging time for 356 alloys containing four levels of Fe, and aged at 180 °C: **a** non-modified alloys, and **b** Sr-modified alloys

dislocations in a phenomenon known as pile-ups. The micro-stresses originating at the interface between the precipitated phase particles and the matrix as a result of dislocation pile-ups intensify the possibility of microcrack initiation at these interfaces [16, 17]. The impact properties were, thus, seen to decrease with further increases in the aging time up to 8 h for both non-modified and Sr-modified 356 alloys, as shown in Fig. 7. Such reduction is thought to be primarily a result of the reduction in the resistance of the matrix to microcrack initiation and propagation.

Increasing the aging time to 12 h, however, results in a slight recovery in the impact energies of these alloys for both cases. Such minor restoration in impact energy values may be ascribed to the coarsening and coherency loosening of the Mg_2Si particles, leading to easy motion of dislocations and alloy softening which increase the ductility of the matrix. The preceding changes in the morphology of Mg_2Si phase may contribute significantly in increasing the energy required for initiating and propagating the microcracks.

These results appear to be in good agreement with those obtained from the work of Nakayama et al. [18] regarding the effects of aging conditions on the impact energy of Al–Si alloys. The authors reported that the behavior of impact energy displays a similar tendency after aging for greater periods of time at 145 °C for both Al–2Si–0.3Mg and Al–7Si–0.3Mg alloys. Tsukuda et al. [19], on the other hand, found that aging either at 120 °C or at 180 °C for further aging time up to 12 h results in a continuous decrease in the impact energy values of Al–6.8Si–0.3Mg–0.2Fe alloy.

It should also be observed from Fig. 7 that the Sr-modified 356 alloys display higher impact energy values than non-modified ones for all aging times, regardless of the iron

Table 5 Effects of Sr-modification and aging times on Charpy impact energy values of 356 alloys containing four levels of Fe, and aged at 220 °C

Alloy code	Aging time (h)	E_T (J)	E_I (J)	E_P (J)	Time to failure (ms)	ACS (mm/ms)
A	2	8.26 ± 0.9	4.8 ± 0.6	3.46 ± 0.3	0.34 ± 0.02	29.4 ± 2
	4	7.96 ± 0.5	4.66 ± 0.4	3.3 ± 0.2	0.37 ± 0.03	27 ± 2.2
	6	7.5 ± 0.6	4.62 ± 0.4	2.88 ± 0.3	0.29 ± 0.01	25.6 ± 1.2
	8	7.6 ± 0.9	4.44 ± 0.5	3.27 ± 0.2	0.37 ± 0.01	27 ± 1.3
	12	11.6 ± 0.9	7.36 ± 0.5	4.24 ± 0.1	0.5 ± 0.02	20 ± 1.4
AS	2	9.78 ± 0.3	5.65 ± 0.2	4.13 ± 0.2	0.30 ± 0.01	33.3 ± 1
	4	8.87 ± 0.7	5.14 ± 0.3	3.73 ± 0.4	0.33 ± 0.01	30.3 ± 1.6
	6	9.32 ± 0.6	4.82 ± 0.3	4.5 ± 0.3	0.61 ± 0.01	16.4 ± 1.3
	8	11.78 ± 0.3	7.7 ± 0.2	4.08 ± 0.1	0.5 ± 0.01	20 ± 1
	12	19.95 ± 0.9	13.55 ± 0.5	6.4 ± 0.4	0.65 ± 0.03	15.4 ± 0.9
B	2	6.98 ± 0.9	3.56 ± 0.5	3.42 ± 0.2	0.38 ± 0.02	26.3 ± 1.7
	4	6.81 ± 0.9	5.14 ± 0.6	1.67 ± 0.3	0.36 ± 0.01	27 ± 1
	6	6.9 ± 0.9	3.98 ± 0.4	2.92 ± 0.3	0.36 ± 0.03	27.7 ± 2.1
	8	7.45 ± 0.9	4.18 ± 0.5	3.27 ± 0.4	0.37 ± 0.05	27 ± 1.5
	12	11.45 ± 0.8	7.17 ± 0.5	4.28 ± 0.3	0.5 ± 0.04	20 ± 1.5
BS	2	8.03 ± 0.9	4.8 ± 0.6	3.23 ± 0.4	0.41 ± 0.02	24.3 ± 1.8
	4	7.08 ± 0.6	3.58 ± 0.4	3.50 ± 0.2	0.39 ± 0.01	25.6 ± 1.3
	6	7.83 ± 0.6	4.03 ± 0.4	3.80 ± 0.2	0.33 ± 0.01	30 ± 1.6
	8	8.81 ± 0.2	5.23 ± 0.2	3.58 ± 0.7	0.39 ± 0.06	25.6 ± 2
	12	14.27 ± 0.3	9.14 ± 0.2	5.13 ± 0.2	0.51 ± 0.01	18.6 ± 0.8
C	2	4.7 ± 0.5	2.49 ± 0.3	2.0 ± 0.2	0.25 ± 0.01	40 ± 1.9
	4	5.48 ± 0.3	2.97 ± 0.2	2.51 ± 0.1	0.29 ± 0.01	34.5 ± 1.2
	6	5.4 ± 0.5	2.86 ± 0.3	2.54 ± 0.2	0.29 ± 0.01	34.4 ± 1.4
	8	5.34 ± 0.2	2.13 ± 0.1	3.21 ± 0.1	0.26 ± 0.01	38.5 ± 1.3
	12	6.9 ± 0.5	3.77 ± 0.3	3.2 ± 0.2	0.35 ± 0.01	28.6 ± 1.2
CS	2	6.88 ± 0.6	4.04 ± 0.4	2.84 ± 0.2	0.30 ± 0.01	33.3 ± 2
	4	6.63 ± 0.2	3.56 ± 0.1	3.07 ± 0.7	0.31 ± 0.04	32.2 ± 3
	6	6.47 ± 0.2	3.43 ± 0.2	3.05 ± 0.1	0.32 ± 0.01	31.2 ± 1.6
	8	6.13 ± 0.7	3.35 ± 0.4	2.78 ± 0.2	0.33 ± 0.01	30.3 ± 2.3
	12	13.06 ± 0.7	8.12 ± 0.7	4.94 ± 0.5	0.48 ± 0.01	20.8 ± 1.7
D	2	3.3 ± 0.4	1.71 ± 0.2	1.6 ± 0.2	0.22 ± 0.01	45.5 ± 1.7
	4	3.27 ± 0.5	1.6 ± 0.2	1.67 ± 0.3	0.23 ± 0.01	43.5 ± 2.5
	6	3.48 ± 0.5	1.8 ± 0.3	1.68 ± 0.2	0.24 ± 0.02	41.6 ± 1.9
	8	3.18 ± 0.4	1.55 ± 0.2	1.63 ± 0.32	0.24 ± 0.01	41.6 ± 2.3
	12	5.18 ± 0.6	2.56 ± 0.3	2.62 ± 0.3	0.31 ± 0.01	32.2 ± 2.4
DS	2	3.80 ± 0.2	2.0 ± 0.1	1.2 ± 0.1	0.23 ± 0.01	43.5 ± 2
	4	3.50 ± 0.6	1.85 ± 0.3	1.65 ± 0.3	0.26 ± 0.02	38.5 ± 3
	6	3.42 ± 0.7	1.71 ± 0.4	1.71 ± 0.3	0.27 ± 0.01	37 ± 2.2
	8	3.76 ± 0.5	1.85 ± 0.3	1.91 ± 0.2	0.25 ± 0.01	40 ± 2.2
	12	6.57 ± 0.5	3.34 ± 0.2	3.23 ± 0.3	0.32 ± 0.01	31.2 ± 0.9

content. These higher values may be attributed to the difference in the characteristics of microstructural constituents between the Sr-modified and non-modified alloys in terms of the morphology and size of both eutectic Si particles and the iron-based intermetallics occurring during solution heat treatment. Since no data were reported in the literature revealing any changes in the morphology and size of the eutectic Si and iron-bearing intermetallic phases during aging treatment, the lowest impact energy values were obtained from both D and DS alloys (0.9 wt% Fe).

Aging at such a high temperature results in the softening of the alloys; this fact is evident from the higher impact energy values listed in Table 5 which were obtained in the case of both non-modified and Sr-modified alloys

compared to those obtained at 180 °C for the same alloys. The effects of matrix-softening on the impact energy values is more pronounced particularly after 12 h of aging when the highest impact energy values are obtained, as may be seen in Fig. 8. The coarsening of the Mg_2Si phase at this over-aging stage facilitates the motion of dislocations and hence eliminates the tendency towards dislocation pile-ups at the interface between the precipitated phase particles and the matrix. The possibility of the initiation of microcracks will thus diminish and the resistance of the matrix would certainly be improved as a result. Furthermore, the beneficial microstructural changes occurring after the application of solution treatment to the Sr-modified alloys also increase the improvement to be observed in both the crack initiation and the crack propagation resistance of the matrix.

All of the above facts contribute significantly to the large impact energy values of about 20 J obtained for the AS alloy after 12 h of aging at 220 °C. Such a considerable improvement in the impact energy values appears superior not only to the corresponding values in the as-cast condition but also to those of the entire range of 356 alloys investigated. It will also be observed from Fig. 8 that the behavior of crack initiation energy displays the same tendency as that of the total impact energy. This observation indicates that all the microstructural changes taking place as a result of the application of Sr-modification together with a T7 temper are more effective and pronounced in

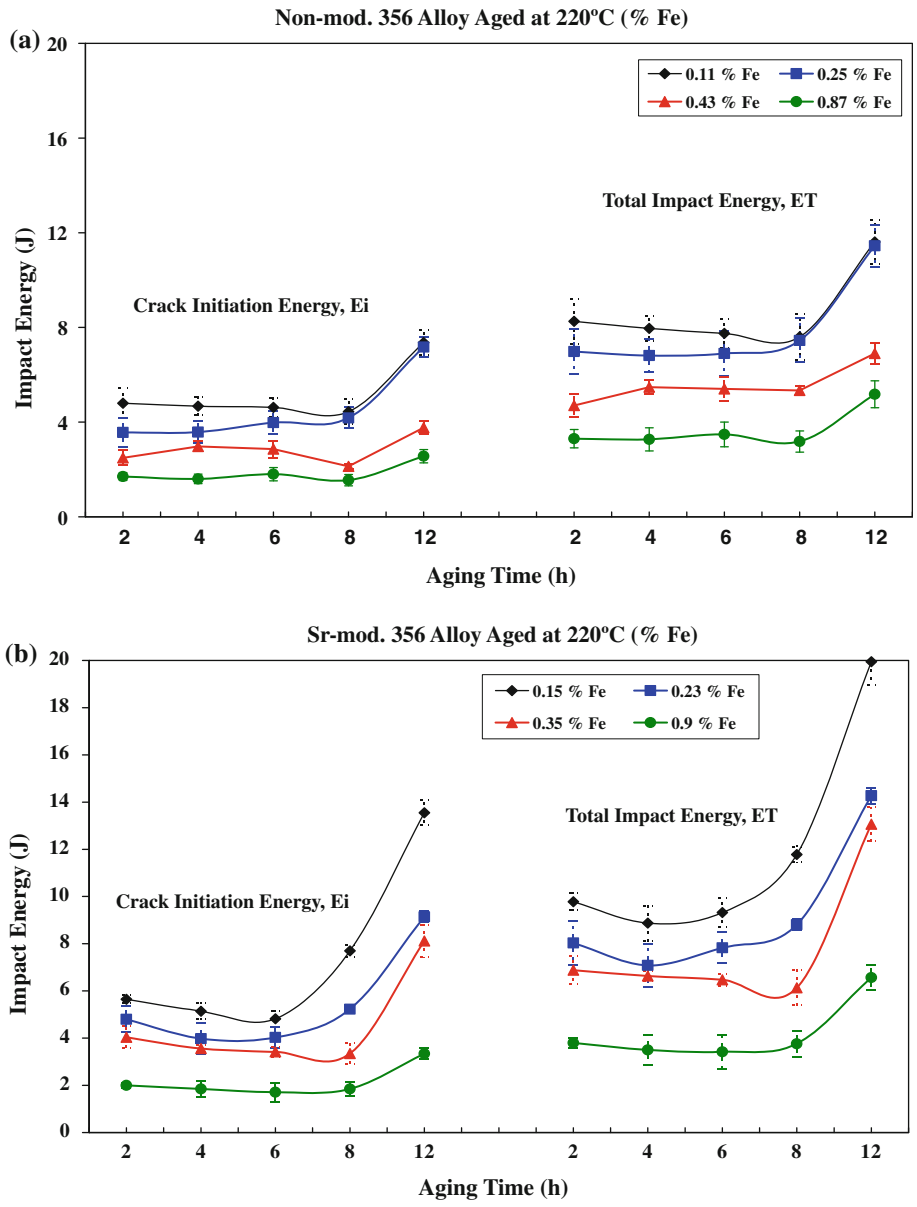

Fig. 8 Impact energy as a function of aging time for 356 alloys containing different additions of Fe, and aged at 220 °C: **a** non-modified alloys, and **b** Sr-modified alloys

improving the CIR of the matrix than they are in conditions of solution treatment and aging at a temperature of 180 °C.

Effects of combined Fe–Mn additions

A number of approaches have been widely reported in previous studies either to reduce or level off the deleterious effects of the β-Fe platelet iron intermetallic phases on the mechanical properties of cast Al–Si alloys [20–22]. One of these approaches involves the addition of neutralizing Mn element where it tends to tie up with Al and Fe so as to form the more compact Chinese script α-Fe intermetallic phase [23]. The average values of different impact parameters and their standard deviations for 356 alloys containing combined Fe–Mn additions in the as-cast and solution heat-treated conditions are summarized in Table 3. Also, it is obvious from Fig. 9 that addition of Sr improves the impact energy values of non-modified alloys as a result of the beneficial size and morphological changes occurring in the eutectic Si phase. This improvement may be ascribed to an increase in the matrix resistance to microcrack initiation as well as to an increase in the proportion of the ductile α-Al phase in the matrix. Applying the T4 treatment appears to improve the impact energy values to a noticeable degree, particularly for both E and ES alloys (0.2 wt% Fe–0.1 wt% Mn), as shown in Fig. 9.

The accelerated spheroidization and coarsening rates of the eutectic Si particles during solution treatment increase the inter-particle spacing and thus, also increase the proportion of ductile α-Al phase which separate the eutectic Si phase particles in the matrix. Such changes in the features of the microstructural constituents lead to a significant improvement in the resistance of the matrix to the crack propagation [14]. The dissolution of the brittle Mg_2Si particles after the application of a T4 temper also increases this improvement. The T4 treatment process thus succeeds in cutting down on as many sources for crack initiation in the matrix as is possible.

It is also worth noting from Fig. 9 that the presence of 0.1 wt% Mn in as-cast non-modified E alloy seems to have no observable effect on the impact energy values as expected, when they are compared to those obtained for the A alloy (0.12 wt% Fe). The precipitation of iron as α-Fe Chinese script particles within α-Al dendrites in this case results in diminishing the amounts of detrimental β-iron platelets, thereby leading to a certain amount of improvement in the resistance of the matrix to CIR. On the other hand, the strengthening effect resulting from the precipitation of α-Fe particles within the dendrites decreases the ductility of the matrix and hence weakens the resistance of the matrix to crack propagation (CPR). It appears that the increase in the CIR values may be negated by the decrease in those for CPR and this balance between the two components of total impact energy may explain the insignificant influence of the addition of 0.1 wt% Mn on the impact energy values of 356 alloys. Increasing the level of Mn addition up to 0.4 wt% (G alloy), however, is observed to slightly improve the impact energy values for both non-modified and Sr-modified alloys compared to D and DS alloys under the same conditions. Although, Kumari et al. [20] carried out an investigation on the effects of Mn addition with other elements on the mechanical properties of Al–7Si–0.3Mg–0.8Fe alloy. Their results indicate that an addition of 0.4 wt% Mn promotes the formation of the Chinese script α-Fe phase. No observable improvement in the impact strength values, however, was obtained for non-modified alloys containing 0.4 wt% Mn; it should be noted that these values appear to be less than those obtained for the as-cast non-modified alloy without any additives.

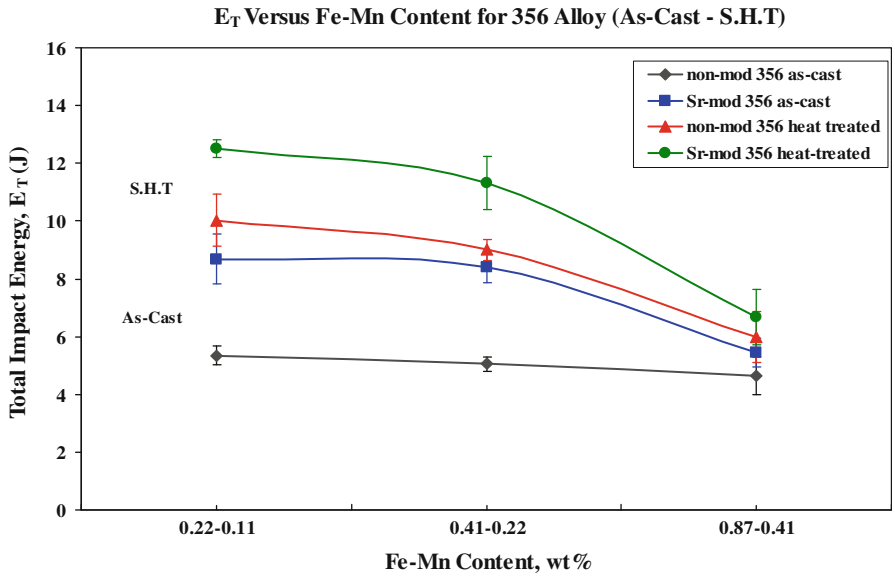

Fig. 9 Total impact energy plotted against Fe–Mn content in non-modified and Sr-modified 356 alloys for the as-cast and solution heat-treated conditions

Table 6 Charpy impact properties of 356 alloys containing various levels of Fe–Mn, and aged at 180 °C for different times

Alloy code	Aging time (h)	E_T (J)	E_I (J)	E_P (J)	Time to failure (ms)	ACS (mm/ms)
E	2	7.35 ± 0.5	3.95 ± 0.3	3.4 ± 0.2	0.29 ± 0.01	34.5 ± 1.4
	4	5.4 ± 0.9	2.93 ± 0.6	2.3 ± 70.3	0.26 ± 0.04	38.5 ± 3
	6	5.35 ± 0.9	2.75 ± 0.5	2.6 ± 0.4	0.27 ± 0.01	37.0 ± 2.4
	8	3.61 ± 0.2	1.77 ± 0.1	1.84 ± 0.1	0.24 ± 0.01	41.6 ± 1.2
	12	5.28 ± 0.3	2.62 ± 0.2	2.66 ± 0.15	0.25 ± 0.01	40 ± 0.7
ES[a]	2	12.2 ± 0.3	7.75 ± 0.4	4.45 ± 0.2	0.47 ± 0.06	21.3 ± 2.8
	4	8.3 ± 0.5	4.47 ± 0.5	3.83 ± 0.5	0.30 ± 0.03	33.3 ± 3
	6	6.28 ± 0.8	3.35 ± 0.3	2.93 ± 0.2	0.31 ± 0.01	32.2 ± 1
	8	5.2 ± 0.7	2.75 ± 0.2	2.45 ± 0.1	0.27 ± 0.01	37 ± 2.1
	12	9.56 ± 0.9	5.37 ± 0.6	4.19 ± 0.1	0.32 ± 0.09	31.2 ± 3
F	2	3.9 ± 0.2	1.9 ± 0.1	1.9 ± 0.2	0.25 ± 0.07	40 ± 1.8
	4	3.47 ± 0.4	1.72 ± 0.2	1.75 ± 0.2	0.22 ± 0.02	45.5 ± 3
	6	3.27 ± 0.5	1.52 ± 0.3	1.75 ± 0.2	0.24 ± 0.01	41.6 ± 1.8
	8	3.24 ± 0.4	1.64 ± 0.3	1.6 ± 0.1	0.23 ± 0.01	43.5 ± 3
	12	4.03 ± 0.9	2.03 ± 0.5	2 ± 0.4	0.25 ± 0.01	40 ± 2.2
FS	2	6.20 ± 0.9	3.47 ± 0.5	2.73 ± 0.7	0.34 ± 0.03	29.4 ± 4
	4	5.02 ± 0.9	2.58 ± 0.5	2.44 ± 0.9	0.33 ± 0.05	30.3 ± 4
	6	4.76 ± 0.9	2.51 ± 0.5	2.25 ± 0.7	0.30 ± 0.02	33.3 ± 3
	8	4.7 ± 0.9	2.48 ± 0 6	2.22 ± 0.4	0.27 ± 0.01	37 ± 3
	12	6.8 ± 0.9	3.52 ± 0.6	3.28 ± 0.6	0.26 ± 0.02	38.5 ± 3
G	2	3.47 ± 0.4	1.73 ± 0.2	1.74 ± 0.2	0.23 ± 0.01	43.4 ± 2.5
	4	2.95 ± 0.8	1.45 ± 0.4	1.5 ± 0.5	0.23 ± 0.01	43.4 ± 1.6
	6	3.09 ± 0.3	1.52 ± 0.2	1.57 ± 0.1	0.22 ± 0.01	45.5 ± 1.4
	8	2.8 ± 0.3	1.23 ± 0.1	1.57 ± 0.2	0.24 ± 0.01	41.6 ± 2.5
	12	3.6 ± 0.4	1.82 ± 0.2	1.78 ± 0.2	0.24 ± 0.01	41.6 ± 1.4
GS	2	5.0 ± 0.6	2.9 ± 0.5	2.1 ± 0.1	0.29 ± 0.08	34.5 ± 4
	4	3.86 ± 0.5	1.86 ± 0.3	2.0 ± 0.2	0.25 ± 0.01	40 ± 2.1
	6	4.31 ± 0.5	2.15 ± 0.3	2.16 ± 0.1	0.26 ± 0.01	38.5 ± 1.14
	8	4.17 ± 0.4	1.96 ± 0.2	2.21 ± 0.2	0.25 ± 0.01	40 ± 1.6
	12	4.37 ± 0.3	2.24 ± 0.2	2.13 ± 0.1	0.24 ± 0.01	41.6 ± 1

[a] S: Sr-modified; see Table 7 for alloy Fe–Mn levels

The addition of Mn to 356 alloys is reported to have no observable influence either on their response to the aging process or on the subsequent precipitation-hardening reactions. Table 6 provides the average values with their standard deviations for the different parameters which were determined from the Charpy impact test for non-modified and Sr-modified 356 alloys containing three levels of combined Fe–Mn additions. It will be observed, from Fig. 10, that the impact energy displays virtually the same type of behavior as that observed in the alloys containing only iron, as shown in Fig. 7. A noticeable improvement in the impact energy values may be obtained for the D alloy after only 2 h of aging compared to those obtained in the as-cast condition for A alloys. This improvement is to be expected since, in this case, the alloys are in the under-aged stage. The impact energy values, thereafter, decline over time to reach a minimum after 8 h of aging in view of the maximum hardness attained during the peak-aging stage.

Increasing the aging time up to 12 h results in a noticeable recovery in the impact energy, particularly for ES alloys (0.2 wt% Fe–0.1 wt% Mn), as may be seen clearly in Fig. 10b which shows the over-aging stage. The changes in the shape of the hardening Mg_2Si phase during the different stages of the aging process thus significantly affect the impact behavior of these alloys. It may be concluded that a third parameter, which is the size and morphology of the Mg_2Si phase, controls the impact energy values mutually with the eutectic Si and iron-containing intermetallic phases in these conditions.

The beneficial changes in the morphology and size of both eutectic Si and iron-based intermetallic phases associated with the addition of Sr and solution treatment may

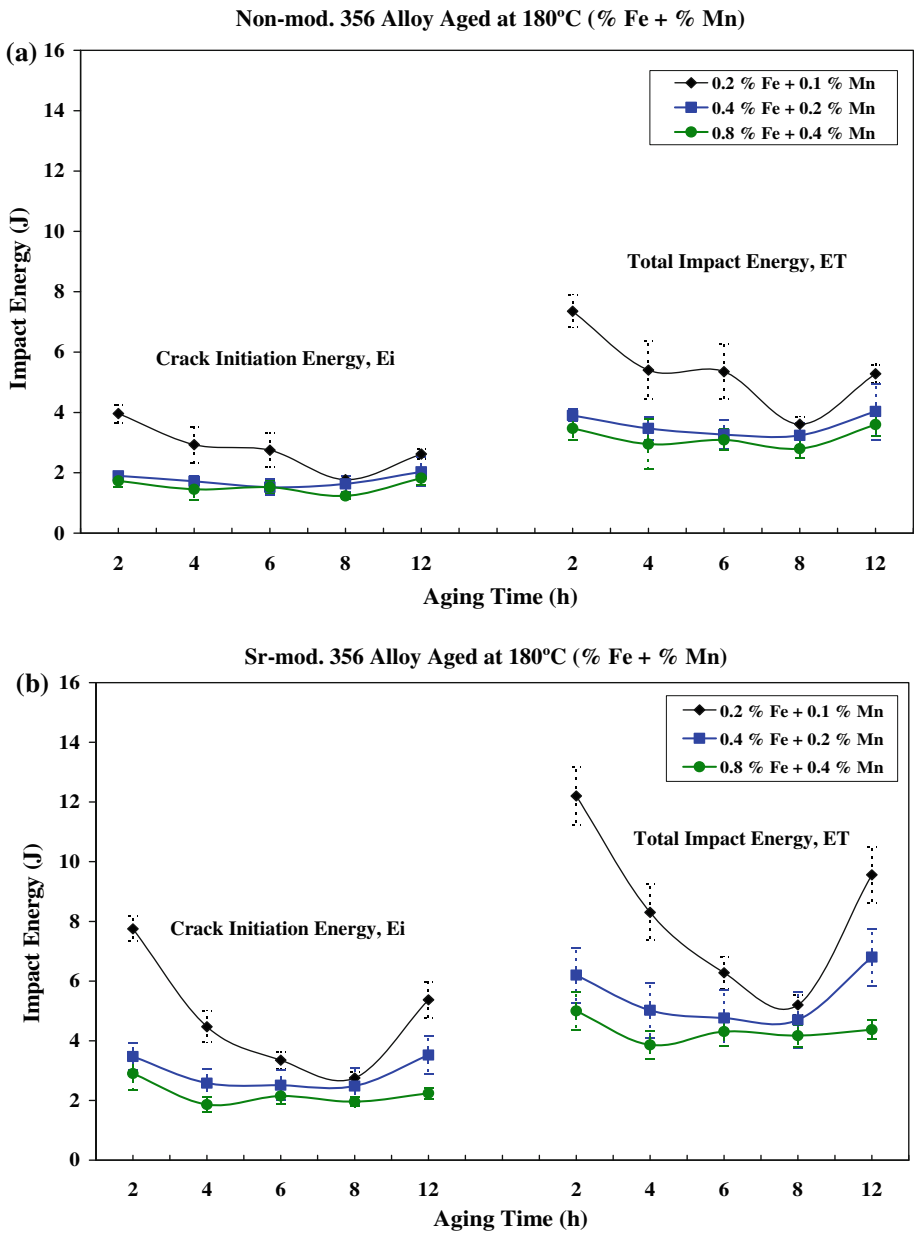

Fig. 10 Impact energy as a function of aging time for 356 alloys containing different combined additions of Fe–Mn, and aged at 180 °C: **a** non-modified alloys, and **b** Sr-modified alloys

explain the relatively higher impact energy values obtained for ES alloy. The influence of the aging treatment on the impact energies of the G and GS alloys (0.9 wt% Fe–0.4 wt% Mn) is not apparent since these alloys possess a higher volume fraction of iron-bearing intermetallic compounds. Consequently, from Fig. 10, it may be assumed that both the size and morphology of the iron-based intermetallic phases are the predominant factors controlling the impact behavior in these alloys. It should also be noted here that the behavior of the crack initiation energy values (E_I) displays the same tendency as that of the total impact energy values (E_T).

Table 7 lists the average values for impact energy with their standard deviations, as well as a variety of other parameters relating to 356 alloys containing three levels of combined Fe–Mn addition, and aged at 220 °C for various aging times. The response of these alloys to the expected softening effect at such high aging temperature is evident from the behavior of the impact energy values shown in Fig. 11. The impact energy values are seen to increase in a virtually linear manner with further aging times of up to 12 h for the non-modified alloys, particularly for the G alloy (0.2 wt% Fe–0.1 wt% Mn), as shown in Fig. 11a. The impact behavior of Sr-modified alloys shows the same tendency as that obtained in non-modified alloys, although they display considerable improvement after aging at 220 °C for 12 h (over-aging stage). The same significant improvement is also observed in the crack initiation energy

Table 7 Charpy impact properties of 356 alloys containing various levels of Fe–Mn, and aged at 220 °C for different times

Alloy code	Aging time (h)	E_T (J)	E_I (J)	E_P (J)	Time to failure (ms)	ACS (mm/ms)
E	2	5.27 ± 0.6	2.73 ± 0.3	2.54 ± 0.2	0.27 ± .01	37 ± 1.2
	4	5.8 ± 0.9	3.02 ± 0.4	2.78 ± 0.5	0.32 ± .02	31.2 ± 2.7
	6	6.8 ± 0.9	3.7 ± 0.5	3.1 ± 0.4	0.35 ± .03	28.5 ± 1
	8	8.89 ± 0.9	5.17 ± 0.4	3.72 ± 0.2	0.45 ± 0.1	22.2 ± 0.7
	12	9.92 ± 0.9	5.82 ± 0.6	4.1 ± 0.4	0.46 ± .03	21.7 ± 1.5
ES[a]	2	6.92 ± 0.3	3.9 ± 0.2	3.02 ± 0.1	0.35 ± .01	28.6 ± 0.8
	4	7.31 ± 0.5	4 ± 0.4	3.31 ± 0.1	0.39 ± .01	25.6 ± 1.7
	6	8.51 ± 0.8	4.73 ± 0.5	3.78 ± 0.3	0.43 ± 0.2	23.2 ± 2
	8	9.7 ± 0.7	5.36 ± 0.5	4.34 ± 0.3	0.42 ± .01	23.8 ± 0.8
	12	18.1 ± 0.9	12.15 ± 0.5	5.95 ± 0.4	0.65 ± .04	15.4 ± 0.1
F	2	4.51 ± 0.4	2.34 ± 0.2	2.17 ± 0.2	0.26 ± .01	38.5 ± 2.4
	4	4.95 ± 0.4	2.60 ± 0.2	2.35 ± 0.1	0.28 ± .01	35.7 ± 1.6
	6	5.23 ± 0.9	2.8 ± 0.5	2.43 ± 0.4	0.29 ± .03	34.5 ± 3
	8	5.83 ± 0.2	3.34 ± 0.4	2.49 ± 0.2	0.32 ± .01	31.2 ± 1.7
	12	6.84 ± 0.9	3.6 ± 0.6	3.24 ± 0.8	0.34 ± .07	29.4 ± 0.1
FS	2	5.88 ± 0.8	3.15 ± 0.3	2.73 ± 0.3	0.32 ± .04	31.2 ± 1.8
	4	6.5 ± 0.9	3.18 ± 0.5	3.32 ± 0.7	0.37 ± .03	27 ± 2.9
	6	7.3 ± 0.9	4.04 ± 0.5	3.26 ± 0.4	0.39 ± .02	25.6 ± 1.7
	8	8.3 ± 0.6	4.97 ± 0.3	3.33 ± 0.3	0.36 ± .01	27.7 ± 0.7
	12	17.1 ± 0.5	11.6 ± 0.5	5.46 ± 0.1	0.62 ± .02	16.1 ± 0.1
G	2	2.6 ± 0.1	1.21 ± .01	1.39 ± 0.1	0.22 ± .01	45.5 ± 1.6
	4	4.16 ± 0.3	2.09 ± 0.2	2.07 ± 0.1	0.25 ± .01	40 ± 1.2
	6	4.66 ± 0.4	2.42 ± 0.3	2.24 ± 0.1	0.27 ± .01	37 ± 2.2
	8	5.09 ± 0.8	2.76 ± 0.5	2.33 ± 0.4	0.26 ± .01	38.5 ± 0.6
	12	6.18 ± 0.8	3.44 ± 0.4	2.74 ± 0.8	0.33 ± .02	30.3 ± 2
GS	2	4.58 ± 0.9	2.38 ± 0.4	2.20 ± 0.5	0.26 ± .02	38.5 ± 4
	4	5.04 ± 0. 9	2.63 ± 0.4	2.68 ± 0.6	0.30 ± .02	33.3 ± 3
	6	5.84 ± 0.4	3.25 ± 0.3	2.59 ± 0.2	0.32 ± .02	31.2 ± 2.7
	8	6.31 ± 0.8	3.56 ± 0.5	2.75 ± 0.3	0.33 ± .024	30.3 ± 3
	12	9.95 ± 0.8	5.65 ± 0.4	4.3 ± 0.4	0.45 ± .04	22.2 ± 0.1

[a] S: Sr-modified; see Table 6 for alloy Fe–Mn levels

values in that they confirm the softening effect occurring in these alloys upon application of the T7 temper.

It may be concluded from the above mentioned results that the aging treatment parameters appears to contribute significantly to either improving or reducing the matrix resistance to crack initiation by also controlling the number of stress concentration sites at the interface between the particles of the precipitated phases and the matrix. The strength and ductility of the α-aluminum phase which affected by the aging treatment will also govern the propagation of the cracks in the matrix. The high impact energies obtained through the application of a T7 treatment in the case of AS alloys (0.15 wt% Fe) or ES alloys (0.2 wt% Fe–0.1 wt% Mn) may be one of the appropriate solutions to be suggested for avoiding any unexpected breakdown occurring in components made from cast 356 alloys due to crash.

Microstructure beneath the fracture surface

A number of longitudinal sections were extracted perpendicular to the fracture surface from selected impact-tested samples of 356 alloys to examine the fracture profile beneath the fracture surface using an optical microscope. This examination was carried out with a view to determining the microstructural constituents which cause and/or contribute strongly to either the crack initiation or crack propagation processes, these being the two main components of the fracture mechanism.

Figure 12 shows optical micrographs of the longitudinal sections below the fracture surface of A alloy samples (0.12 wt% Fe), and aged for 12 h at 180 °C. It will be observed from these micrographs that the formation of microcracks begins with the cracking of the brittle acicular eutectic Si particles. During the impact testing, rapid

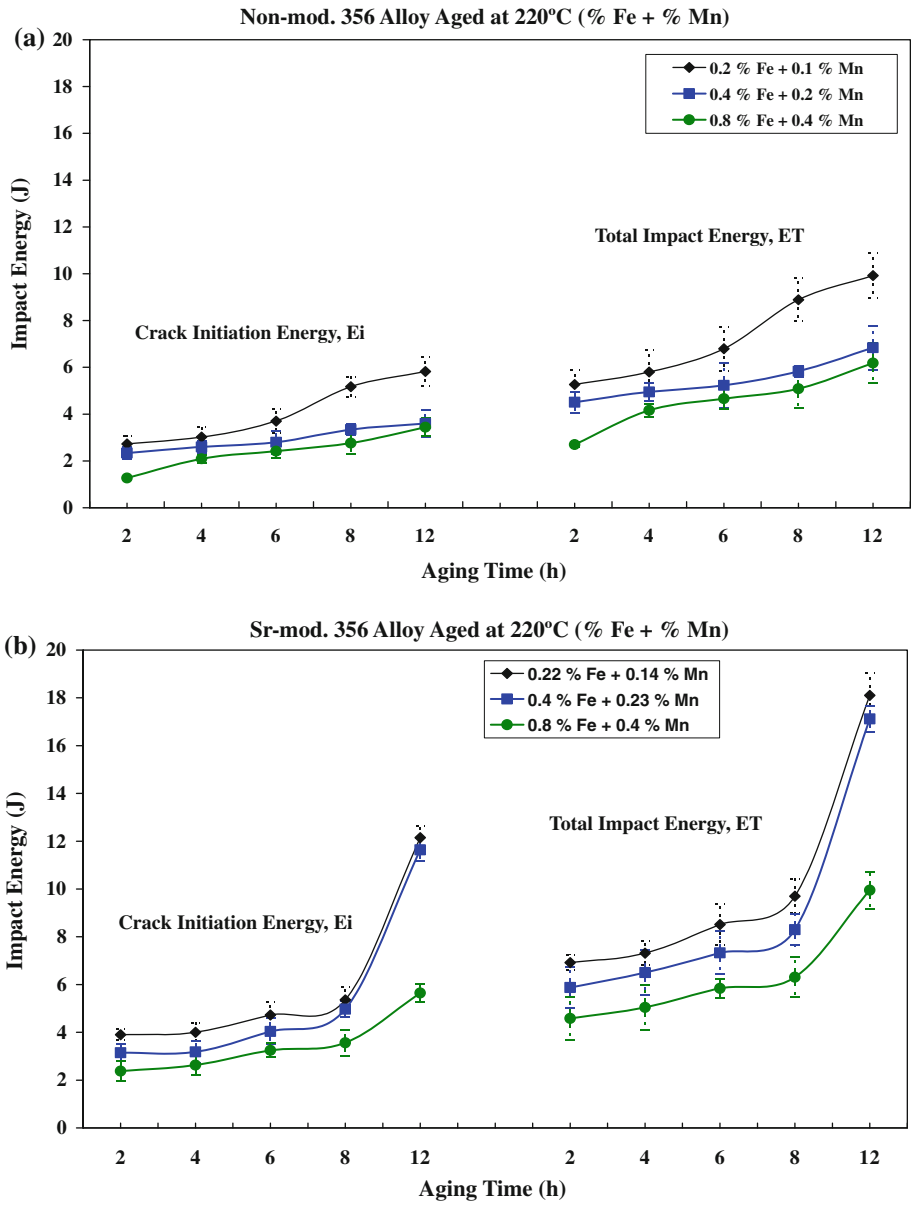

Fig. 11 Impact energy as a function of aging time for 356 alloys containing different additions of Fe–Mn, and aged at 220 °C: **a** non-modified alloys, and **b** Sr-modified alloys

non-homogeneous deformation induces internal stresses on the eutectic Si particles and Fe-based intermetallics which start to crack once these internal stresses reach the level of the fracture stress of these particles [24, 25]. In Fig. 12a, a secondary microcrack is also observed in the β-iron platelet in the microstructure under the fracture surface. Such an observation confirms the lower impact energy values of about 5.5 J obtained for A and AS alloys under the same aging conditions. Once a large number of eutectic Si particles crack, the microcracks start to grow by linking with adjacent microcracks formed by fracture of other particles so as to form one principal crack. The crack then continues to propagate through the cleavage of other acicular Si particles along the direction shown in Fig. 12b, where the fracture appears to display a mainly brittle mode.

The fracture profile beneath the fracture surface of AS alloys aged at 180 °C for 12 h is shown in Fig. 13. The edge of the sample indicated by the arrow at the left seems to be more curved or rounded than the same area observed in the non-modified alloys (Fig. 12a). The fracture surface also shows separation of the α-Al dendrites indicating that the fracture occurs primarily in a ductile mode, as may be seen clearly in Fig. 13a. The principal crack is then formed by the local linkage of adjacent microcracks. The crack subsequently propagates via further cleavage of both π- and β-iron intermetallic phases and the fracture path goes mainly through the interdenritic regions, as shown by the arrows in Fig. 13b, displaying an intergranular fracture mode.

Figure 14 represents optical micrographs of the fracture profile beneath the fracture surface, obtained from

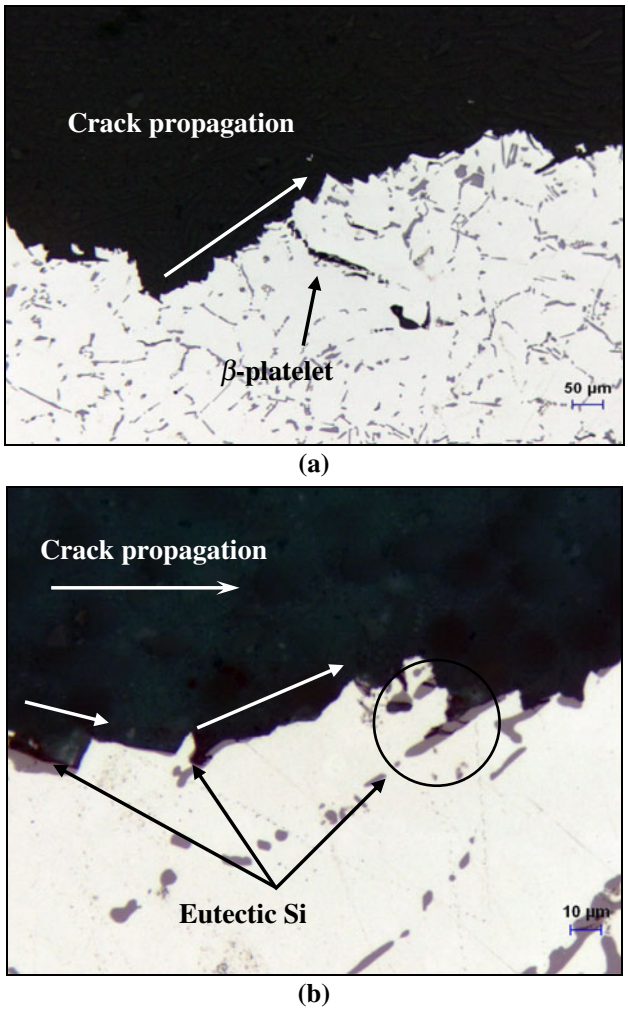

Fig. 12 Optical micrographs obtained from longitudinal sections below the fracture surface of non-modified 356 alloy samples containing 0.1 wt% Fe, and aged for 12 h at 180 °C showing the brittle fracture by cleavage of **a** a β-iron platelet, and **b** cracking of eutectic Si particles

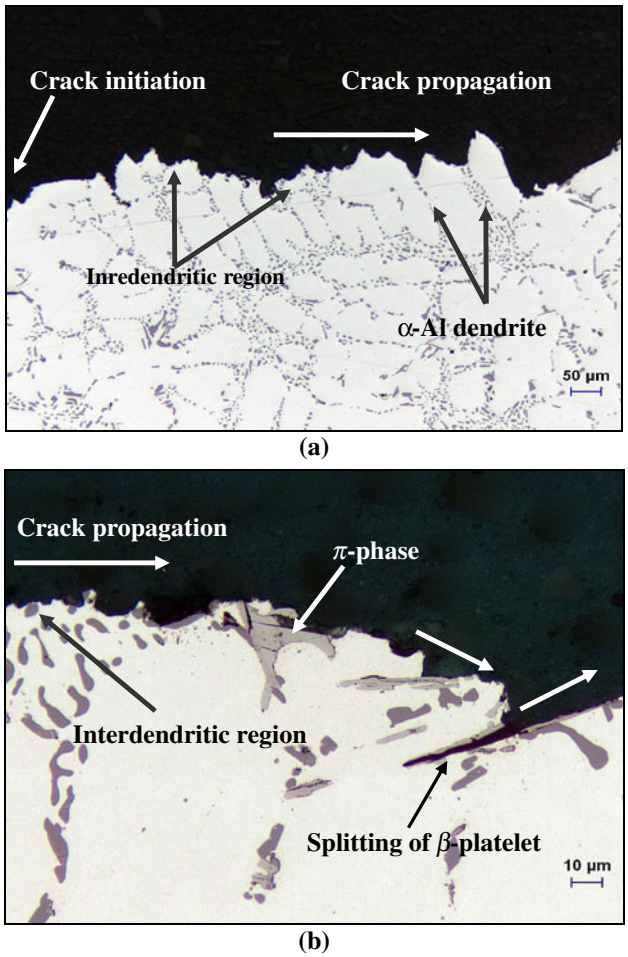

Fig. 13 Optical micrographs of Sr-modified 356 alloy containing 0.1 wt% Fe showing crack propagation: **a** through interdendritic regions, and **b** via cracking of β-iron platelets and π-iron phase particles

longitudinal sections of impact-tested 356 alloy samples. This figure shows the role of iron-based intermetallic phases in the fracture process of both D and G alloys. It is apparent that the fracture profile is mainly flat and straight, indicating that the fracture displays a brittle mode. The fracture of long β-iron platelets contributes strongly to the propagation of microcracks, as shown in Fig. 14b which is a high magnification view of the encircled area shown in Fig. 14a. Also, secondary microcracks may form by the splitting of the β-iron platelet into two halves through the middle. The stresses located at the front of this crack are relaxed by local plastic flow into the surrounding ductile α-Al matrix, halting the propagation of the crack. This observation confirms the fact that β-iron platelet are increasingly susceptible to fracture because of their high aspect ratio; it is also in agreement with the approach that larger and elongated particles are more likely to crack than smaller and more rounded ones. Such a fact may also be attributed to the presence of higher internal stresses generated around the elongated particles, thus leading to the probability that cracking will be intensified [26].

The α-iron Chinese script phase, on the other hand, undergoes fracture through its arms, the fracture occurring in a direction parallel to the direction of the striking load during the impact test, as shown in Fig. 14c and d, for GS alloy. The cracking of Chinese script α-Fe particles and its subsequent contribution to crack propagation supports the lower improvement obtained in the impact energy of these alloys. The platelet β-iron particles appear to be present in these alloys in low amount, however, they were also observed to undergo cracking inside the microstructure near the fracture surface, as shown in Fig. 14b, contributing indirectly to the fracture process.

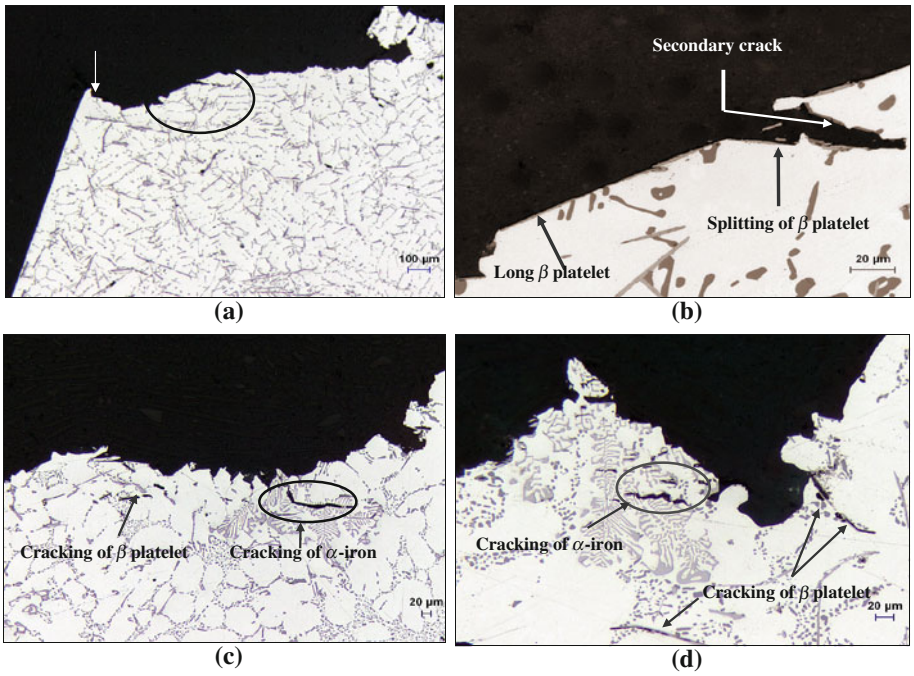

Fig. 14 Optical micrographs showing the effects of iron-based intermetallics on the fracture behavior of 356 alloys: **a**, **b** non-modified alloy containing 0.8 wt% Fe; **c**, **d** Sr-modified alloy containing 0.8 wt% Fe–0.4 wt% Mn

Conclusions

The effects of Sr-modification, iron-based intermetallics and the aging treatment on the impact energy of 356 alloys containing individual Fe additions and combined Fe–Mn additions were investigated. From the results and discussion the following conclusions may be drawn:

1. Increasing the level of Fe addition diminishes the impact energy values of the 356 alloys to a noticeable degree (from ~35 to ~57%), regardless of alloy condition.
2. Combination of Sr-modification and solution treatment significantly improves the total impact energy values (~110%) of the as-cast 356 alloys, particularly at low Fe addition.
3. With respect to aging treatment at 180 °C:
   (i) Impact energy values increase by ~30% at 180 °C/2 h compared to those exhibited by the as-cast alloys;
   (ii) Subsequently, the impact energy decreases with aging times of up to 8 h;
   (iii) A slight recovery in impact energies is observed for the non-modified and Sr-modified alloys after 12 h of aging.
4. The Sr-modified 356 alloys show higher impact energy values compared to non-modified alloys in the same conditions, regardless of the level of Fe addition or combined Fe–Mn additions.
5. The addition of Mn to non-modified 356 alloys seems to have no observable effect on the impact energy values, particularly when compared to the values obtained for the same alloys containing only Fe.
6. From the design and selection point of view, sudden failure may be circumvented through the application of a T7 treatment at 220 °C for 12 h for Sr-modified 356 alloys containing 0.12 wt% Fe or a combined 0.2 wt% Fe–0.1 wt% Mn addition, providing impact energy values of about 20 and 18 J, respectively.
7. The fracture behavior appears to be more controlled by the eutectic Si particles in the non-modified 356 alloys containing 0.12 wt% Fe.
8. The β-iron platelets undergo cracking in the non-modified 356 alloys containing 0.9 wt% Fe providing another source for microcrack initiation and further paths for propagating the cracks. The brittle nature of these platelets is evident from the optical micrographs showing the microstructure beneath the fracture surface.
9. Both π- and β-iron intermetallics contribute significantly to the nucleation and propagation of cracks in the Sr-modified 356 alloys containing 0.12 wt% Fe.

Acknowledgements Financial and in-kind support received from the Natural Sciences and Engineering Research Council of Canada (NSERC), General Motors Power Train Group (USA), and Corporativo Nemak (Mexico), is gratefully acknowledged. The authors would also like to thank Mr. Lang Shi of the Microanalysis Laboratory, Earth and Planetary Science, McGill University for carrying out the EPMA analysis.

References

1. Samuel AM, Samuel FH, Doty HW (1996) J Mater Sci 31:5529. doi:10.1007/BF01159327
2. Bäckerud L, Chai G, Tamminen J (1990) Solidification characteristics of aluminum alloys. Vol. 2: foundry alloys. AFS/Skanaluminium, Des Plaines, IL, p 71
3. Taylor JA Cooperative report, research center for cast metals manufacturing (CAST). University of Queensland, Brisbane, Australia, p 1
4. Paray F, Gruzleski JE (1994) Cast Met 7(1):29
5. Martin JW, Doherty RD (1997) Stability of microstructure in metallic systems. Cambridge University Press, Cambridge, p 239
6. El Sebaie O, Samuel FH, Samuel AM, Doty HW (2008) Mater Sci Eng A 480(1–2):342
7. Taylor JA, StJohn DH, Barresi J, Couper MJ (2000) Mater Sci Forum 331–337:277
8. Taylor A, StJohn DH, Zheng LH, Barresi J, Couper MJ (2001) Alum Trans 4–5:111
9. Wang QG, Davidson CJ (2001) J Mater Sci 36:739. doi:10.1023/A:1004801327556
10. Ma Z, Samuel AM, Samuel FH, Doty HW, Valtierra S (2002) AFS Trans Paper 03–101:1
11. Sigworth G, Apelian D, Shivkumar S (1989) AFS Trans 97:811
12. Shivkumar S, Wang L, Keller C (1994) J Mater Eng Perform 3:83
13. Merlin M, Timelli G, Bonollo F, Garagnani GL (2009) J Mater Process Technol 209:1060
14. Gruzleski JE, Closset BM (1990) The treatment of liquid aluminum–silicon alloys. American Foundrymen's Society, Des Plaines, IL, p 74
15. Zhang DL, Zheng LH, StJohn DH (2002) J Light Met 2:7
16. Dieter GE (1986) Mechanical metallurgy. McGraw Hill, UK, p 241
17. Smallman RE, Ngan AHW (2007) Physical metallurgy and advanced materials. Butterworth Heinemann, Boston, p 385
18. Nakayama Y, Ninomiya K, Ohnishi N (1998) J Jap Inst Light Met 48(7):340
19. Tsukuda M, Koike S, Harada M (1978) J Jap Inst Light Met 28(1):8
20. Sreeja Kumari SS, Pillai RM, Pai BC (2007) Mater Sci Eng A 460–461:561
21. Sreeja Kumari SS, Pillai RM, Pai BC (2002) Indian Found J 48(1):27
22. Awano Y, Shimizu Y (1990) AFS Trans 98:889
23. Murali S, Raman KS, Murthy KSS (1994) Int J Cast Met Res 6(4):189
24. Wang QG, Cáceres CH (1998) Mater Sci Eng A A241:72
25. Brooks CR, Choudhury A (1993) Metallurgical failure analysis. McGraw-Hill Inc., New York
26. Ran G, Zhou JE, Wang QG (2008) J Mater Process Technol 207:46